IV International Conference on Particle-based Methods – Fundamentals and Applications
PARTICLES 2015
E. Oñate, M. Bischoff, D.R.J. Owen, P. Wriggers & T. Zohdi (Eds)

VERTICAL NATURAL MODES OF THE GRAVEL AGGREGATE IN THE BALLASTED RAILWAY TRACK

AKIRA AIKAWA

PhD, Senior Researcher, Railway Dynamics Division,
Railway Technical Research Institute
Hikari-cho, Kokubunji, Tokyo, 185-8540 Japan
E-mail: aikawa.akira.11@rtri.or.jp, web page: http://www.rtri.or.jp/

Key words: Ballasted Track, Natural Frequency, Large-scale Parallel Computing, FEM.

Abstract. This research investigates the natural vibration characteristics of the ballast layer by using field measurement, full-scale experiments and large-scale finite element analysis. The results indicate that the natural frequency of the vertical elastic vibration of the ballast layer is numerically detected at around 310 Hz at which the whole ballast aggregate repeats the vertical expansion and shrinkage elastically, and that the rigid-body natural vibration numerically occurs approximately at 120 Hz at which the mass of the track structure vibrates simultaneously up and down as depending on the stiffness of the ballast layer. The stress acting on an angularity part of the ballast gravel is inferred to be about 1100 times greater than the average stress on the bottom surface of the sleepers.

1 INTRODUCTION

The dynamic loads by trains are transmitted to the ballasted layer as an elastic wave through the inside of gravel and consequently induce the natural vibration modes in the ballast layer, specific to the ballast structures, which will trigger the ballast degradation. Therefore, the ballasted track requires periodic maintenance work, which is an important subject of technical research. However, the dynamic characteristics of the ballast layer have not yet been sufficiently elucidated. The dynamic loads are roughly divided into two major factors. One is dynamic load exerted by the passing axle load of a train. The frequency characteristics depend on the number of axes passing per unit of time, and are limited to a low-frequency domain, ranging from only several Hertz to approx. 20 Hz. The other is the impact load generated by the rolling contact mechanism between the wheels and rails. When the sharp-pulse-shaped waveform of the impact load is transformed into a frequency domain, it has many vibration components with broadband characteristics ranging between a low frequency and several kilohertz frequencies. This paper presents the field measurement of the dynamic responses of the ballasted track with a train passing, at a sampling frequency of 10 kHz without low-pass filters, using the special sensing sleepers and sensing stones, which were developed by the authors (Aikawa, 2012); (Urakawa & Aikawa et al, 2009). Moreover, by introducing the finite element transient response analysis of large-scale parallel-computing by FrontISTR (Okuda) based on a fine ballast aggregate model, both of the elastic natural vibration and the rigid-body natural vibration of the granular ballasted layer can be numerically simulated.

2 IDENTIFICATION OF NATURAL VIBRATION MODES THROUGH FULL-SCALE TESTING

2.1 Vertical natural vibration motions

Figure 1 shows the characteristics of the principal natural vibration motions in the vertical direction of the ballast layer. One is the rigid-body natural vibration and the other is the elastic natural vibration. The structure of the ballasted track can be regarded as a single degree of freedom system consisting of sleepers, rails, etc., which constitute the mass of the track structure and also the stiffness of the ballast layer and road bed. The rigid-body vibration is the motion in which this single degree of freedom system vibrates vertically and rigidly under the dynamic load of a train. There are six kinds of rigid-body natural vibration in total: Translational and rotational along each of three axes. However, the translational vibration components in the vertical direction are dominant both in the dynamic loads applied to the ballast layer and in the responses of the ballast layer. Therefore, this research focuses on the translational behavior in the vertical direction. It has been said that this mode exists approx. at 100 Hz (Grassie et al, 1993).

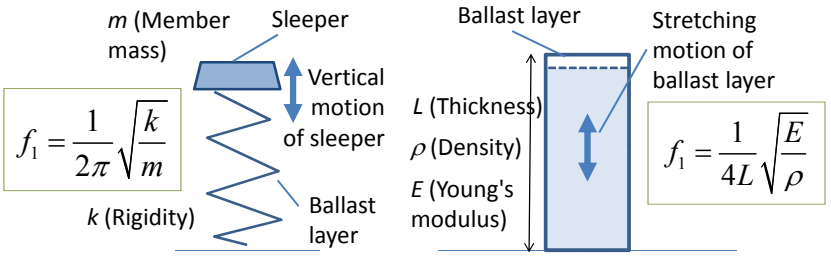

(a) Rigid-body natural vibration (b) Elastic natural vibration

Figure 1: Vertical natural vibration motions

On the other hand, the elastic vibration is the motion in which the whole ballast layer expands and contracts vertically as an elastic body. This natural vibration is considered not to occur in a normal-state ballast layer but to occur when the ballast layer is under high confining pressure generated by the train's weight applied to the ballast layer. So far no research has been done to capture this mode, i.e. ballast motion in the frequency domain related to this mode. It should be added that on a real track natural vibration that entails the bending deformation and torsional deformation of the members occurs.

2.2 Vibration test of a full-scale mockup of a ballasted track

The author built a full-scale mockup of a ballasted track structure and investigated the natural vibration characteristics of a ballasted track by performing an experimental modal analysis based on the impulse excitation test (Sakai & Aikawa et al, 2012); (Aikawa et al, 2011). Figure 2 shows the profile/plane of the mockup and the sensor positions. To build the full-scale mockup, the author employed new ballast using hard Andesite which complies with the same standard for the real track and they were compacted sufficiently. For the mockup, type-3 pre-stressed concrete (PC) mono-block sleepers were used, which are widely used for the meter-gauge (1067 mm wide) conventional railway lines of Japan Railway Companies. The test was performed by vibrating (by hitting) the end of the sleeper with an impulse hammer in three different directions: vertically, laterally and longitudinally. The test record includes the acceleration responses at 22 points on the top surface of the sleeper and several points in the ballast layer. The author then obtained the accelerances, which are the transfer

functions of the acceleration responses to the excitation force in the frequency domain, conducted an experimental modal analysis in consideration of the location relationship of measuring points, and thus identified the natural vibration frequencies and their modal shapes of the ballasted track between the low frequency domain and 1 kHz.

Figure 3 shows the natural vibration frequencies and the specific modal shapes of the ballasted track. Though there are 6 rigid-body vibration modes as stated above, the figure shows only the rigid-body translational mode in the vertical direction and indicates that the vertical, translational rigid-body vibration is generated at 98 Hz, which almost agrees with the previous research results. Besides, 6 types of dominant natural vibration entailing the bending and torsional deformations of sleepers are identified. However, the author was not able to capture any vertical elastic natural vibration of the ballast layer in this test. That is probably because the elastic vibration modes of the whole ballast layer would occur only when continuity in the ballast layer is sufficiently satisfied according to the train loads on the ballast layer.

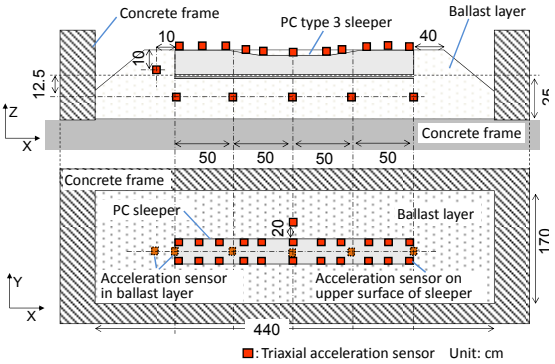

Figure 2: Overview of full-scale test

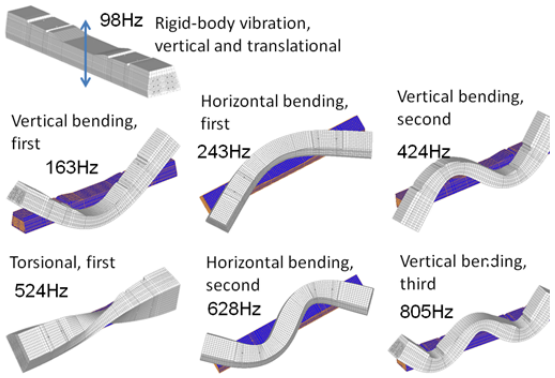

Figure 3: Mode shapes of natural vibration

2.3 Field measurement and spectral analysis

The dynamic responses were measured on an actual ballasted track of a main conventional railway line in Japan. The track structure at the measurement site, consisting of continuous welded rail weighing 60 kg/m and type-3 PC sleepers, was designed based on the Japanese standard (Railway Bureau, MLIT, Japan & RTRI, 2012) that allows a running speed higher than 130 km/h and the measurement site was located on a solid embankment in a straight section. For spacing between the sleepers, 41-42 sleepers are positioned over a distance of 25 m. The ballast layer at the measurement site is made of relatively new Andesite hard gravel with clear-cut edges, and the ballast layer is approx. 30 cm thick. This paper focuses on the measured responses for a train at a traveling speed of approx. 120 km/h with the sampling frequency is 10 kHz. The details of the measurement are described in Reference (Aikawa, 2012).

Figure 4 shows the response acceleration amplitude spectrum and the response displacement amplitude spectrum of the ballast at a depth of 10 cm by applying the fast Fourier transformation of the time history response waveforms, and smoothing them at a bandwidth of 20 Hz. The acceleration spectrum indicates that the high-frequency components above 100 Hz as well as the low-frequency components contribute greatly to the ballast response. When focusing on the ballast displacement, its amplitude is extremely small in the high-frequency domain. For instance, the displacement amplitude is only 1/1000 μm at a frequency of approx. 800 Hz, which is equivalent to the natural frequency of the ballasted track entailing the third mode of the vertical bending of the sleeper. This means that the vibration components in the high-frequency domain are not transmitted by rigid-body vibrations around the center of gravity of the ballast gravel, but the dynamic loads are transmitted through the elastic undulation propagation attributable to the local and minute deformation behavior and sliding behavior at the tips of the edges at the contact points between the ballast stones. On the other hand, the displacement amplitude in the low-frequency domain from several Hertz to 20 Hz is several thousand times larger than those in the high-frequency domain. Consequently, the loads in the low-frequency domain are mainly transmitted through the rotational and/or translational rigid-body vibrations of the individual ballast gravel. This figure also shows the peak profiles of the responses related to the natural vibration modes of the ballasted track, which are shown in the preceding paragraph. These curves identify the rigid-body resonance vibration of the ballast layer around 100 Hz and indicate another large peak profile of the resonance mode around 300 Hz.

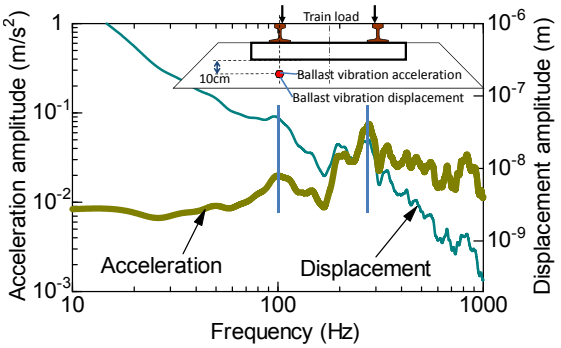

Figure 4: Acceleration and displacement amplitude spectrum of the ballast

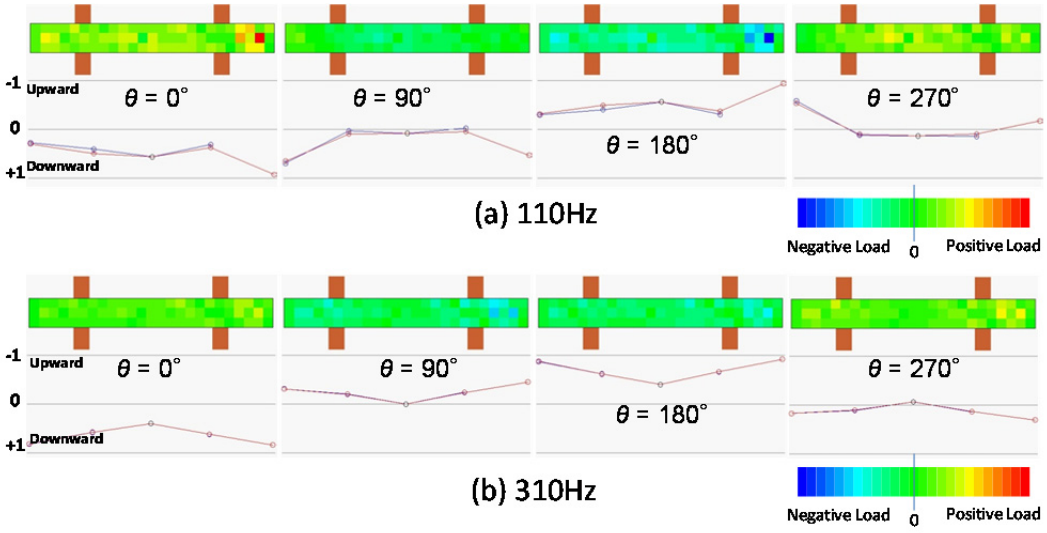

Figure 5: Distribution of the vertical loading at the bottom of the sensing sleeper and the normalized displacement at the top of the sleeper (measured)

Figure 5 shows the relationship between the vertical loading on the bottom surface of the sleeper and the normalized vertical displacement of the sleeper in cases of two different frequencies (110 Hz and 310 Hz). In the figures, θ denotes the relative phase angles. Regarding the sleeper motion, the downward direction indicates the downward behavior of the sleeper and the upward direction indicates the upward behavior of the sleeper. Both the figures (a) and (b) show that the sleeper repeats a vertical periodic movement at these frequencies, with entailing the bending deformations of the sleeper in the high frequency regions, in synchronization with the phase angles.

3 LARGE-SCALE FINITE ELEMENT TRANSIENT RESPONSE ANALYSIS REGARDING THE ELASTIC VIBRATION MODE OF THE BALLASTED TRACK

3.1 Finite element modelling of the ballast aggregate

The three-dimensional shape measurement was performed to determine the three-dimensional vertex coordinates of the ballast gravel. Based on the measured coordinates, each shape was expressed using a polyhedron rigid-body discrete model and converted into an aggregate, with the same size and shape, of tetrahedron secondary elastic finite elements. The details of the measurement are described in reference (Aikawa, 2012).

Figure 6 shows exemplary pictures of a piece of ballast gravel and its numerical discrete element and finite element models. A sufficiently fine mesh size of 1 cm was adopted to support the precise representation of natural frequencies of individual ballast gravel up to several 10 kHz. Table 1 presents the physical property values of the ballast. As the density of the ballast gravel, the laboratory experimental value obtained from specific gravity tests was provided. Young's moduli and Poisson's ratio were derived from the previous reports in the literature. Regarding the structural damping coefficient, the author adopted the general values of a concrete structure.

Figure 7 shows the procedure for the creation of a ballast aggregate by both of the discrete element and finite element modelling. First, about 100 pieces of the ballast polyhedron discrete element models were placed randomly in the air above rectangular box frames. The gravel was then dropped freely by the gravity and compressed vertically with a loading plate

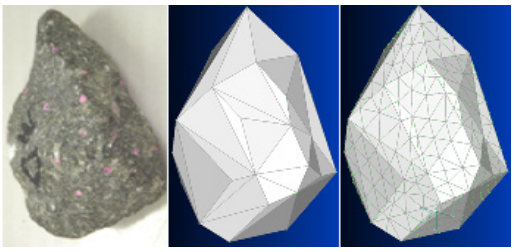

(a) Ballast (b) DEM Model (c) FEM Model

Figure 6: Exemplary pictures of existing ballasts and the digitized models

Table 1: Physical property values

Item	Ballast
Density ρ	2700 (kg/m^3)
Young's modulus E	30 (GPa)
Poisson's ratio ν	0.2
Structural damping parameters η	0.01

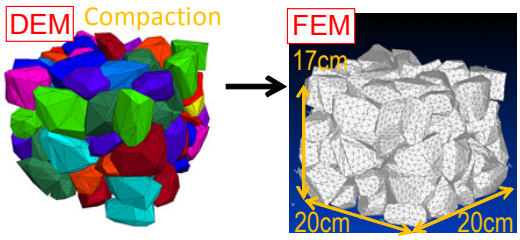

Figure 7: Modelling of the ballast aggregate

using the discrete element software. Next, all individual polyhedron discrete element models were converted into assemblages consisting of the small finite element tetrahedron second-order elastic solid elements, split into 1-cm meshes with geometry and contact-point information maintained. Each polyhedron discrete element model was divided into approximately one thousand tetrahedron finite elements. The finished rectangular block model is 20 cm in width/length and 17 cm in height, and has more than 90 000 tetrahedron finite elements.

In this procedure, the contact-points were connected to one another through Multi-Point Constraints (MPCs), which connected the nodes of elements in three axial directions related to the contact pair of blocks at each contact point. The provided contact-connectivity exhibits no expansion or contraction because its stiffness is several ten thousand times harder than that of ballast pieces. Accordingly, the spring functions around the contact points are represented by the elastic deformation of ballast angularities, which are composed of assemblages of several tetrahedron-finite-elements adjacent to the contact points.

Regarding the modelling of the contact structure, three types of connections were employed according to the mechanism of the connection obtained by the discrete element analysis. The ballast grains touching one another at a single point were linked through one contact location on each stone, and this type of connection allows the rotational behaviors of ballast grains around the contact points. The ballast grains touching one another with their edges were linked through two points at both ends of the side on each stone, and these types of connection between ballast grains allow the rotational behavior of hinge mechanism like a door hinge. The ballast grains touching one another with their faces were linked through three or more points around the contact surface of each stone and these types of connections contribute to the stability of the structure and the propagation of elastic-waves.

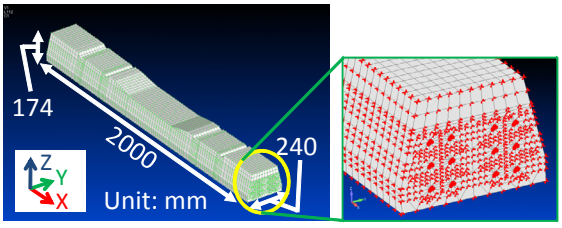

Figure 8: Model of a type 3 PC sleeper

Figures 8 show the finite element model of a type-3 PC sleeper, which is developed by the authors (Sakai & Aikawa et al, 2012) and which consists of 51 146 nodes and 51 944 solid elements. The sleeper model has an ability to make the precise representation of all natural frequencies and their response values up to 1 kHz within 5% deviation. Its physical weight is 161.40 kg and its volume is 0.0677 m^3.

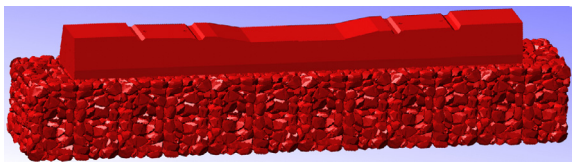

Figure 9: Assembly of ballasted track model

A large-scale finite element model was constructed, with multi-point constraints (MPCs), by assembling 48-units of the above-mentioned rectangular unit block models of the ballast and the type-3 PC sleeper model. Figure 9 shows

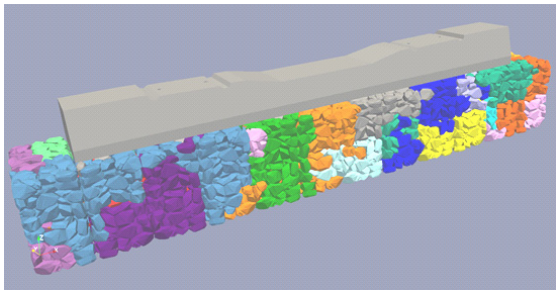

Figure 10: Domain segmentation

the finished analysis model of the sleeper-ballast layer system, which consists of 7.05 million nodes and 4.15 million 2nd order solid elements. The degree of freedom exceeds 21 million. Figure 10 shows the domain segmentation. The whole model is divided into 24 sub-domains for large-scale parallel computing of FrontISTR, by introducing the direct solver MUMPS. By adopting the finite element analysis regarding the modeling of the ballast layer having a complicated structure, it is possible to reproduce the phenomena such as the stress-concentration and the wave-propagation within the ballast layer fast, easily and exactly.

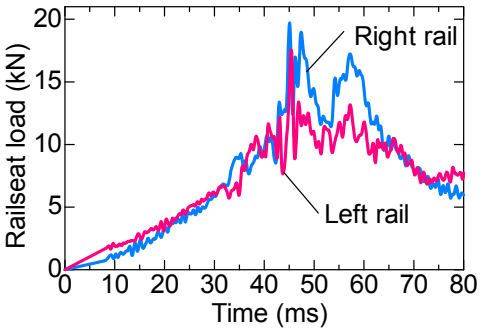

Figure 11: Measured waveform

Table 2: Calculation parameters

Item	Young's modulus (GPa)	Poisson's ratio	Density (kg/m^3)
Ballast	30	0.200	2 700
Concrete	45	0.167	2 350
Steel	210	0.290	7 820

The time-history response waveforms were calculated numerically by inputting measured loading waveforms to the top surface of a sleeper model when a passenger train moved over the top surface of the previously described ballasted track model. Figure 11 shows the actual waveforms of vertical loading (measured in the cross-sectional area 14 cm in width and 18 cm length on the bottom surface of the rails) applied by the first axles of a lead coach bogie when the passenger train moved through the test section at about 120 km/h. In the finite element analysis, the waveforms were uniformly input to the whole points located within the bottom area of the rails on the top surface of the sleeper model. The calculation time interval was set at Δt = 0.1 (ms) and total calculating steps are 800 times. The specifications about the various parameters of each model are shown in Table 2.

3.2 Nodal displacement distribution in the ballast aggregate and the sleeper system

Figure 12 shows the distribution of the nodal displacement in the ballast aggregate and the sleeper system at t = 55.0 (ms) when the load peaks appear as the first axle of the lead coach bogie passed above the sleeper center. It can be seen that the dynamic displacement induced by a passing train on the ballast is not distributed uniformly throughout the ballast aggregate and the sleeper. Significant displacement is concentrated locally around the rail positions. The analytical results show that the 30 μm maximum downward displacement occurred.

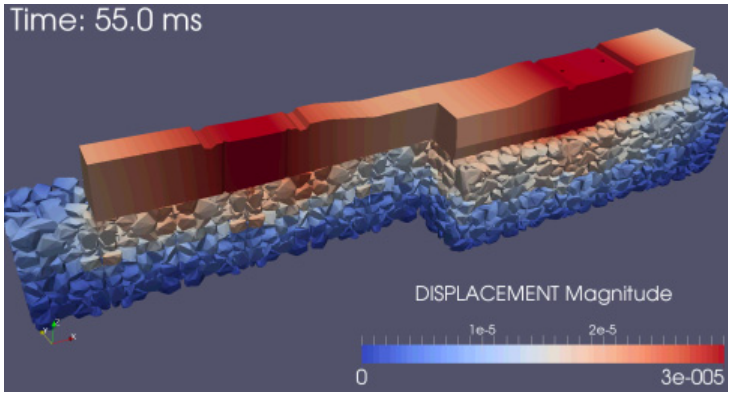

Figure 12: Nodal displacement (t = 55.0 ms)

3.3 Time history of von Mises stress

Figure 13 shows the time history waveforms of response of von Mises stress on the cross-section inside the gravel angularity acting on three different contact points, each with an angularity, of the ballast gravel placed at different depths below the loading point of the left rail location. From the figure, the stresses in the gravel increase gradually, with repeating alternately the minute upward (compression) and downward (tension) motions at the frequency of approximately 300 Hz, according to the inputted loads. In this case, the maximum stresses of approximately 50 MPa after the elapse of about 45 ms to 53 ms are observed near the ballast surface beneath the sleeper bottom. It can be seen that the rise in the peak response value becomes gentler as the measurement point becomes farther (i.e. deeper) from the loading point, and that there is a tendency for waveforms to become smoother along with the steep decrease in high-frequency vibration included in the wave. Although the investigation reported here involves elastic body analysis without the use of any constitutive equations, the diminishing trend of energy inside the ballast is closely reproduced by simulating the actual structure of the ballast aggregate in detail. This means that the ballast aggregate structure featuring angularity parts has the mechanism of energy attenuation.

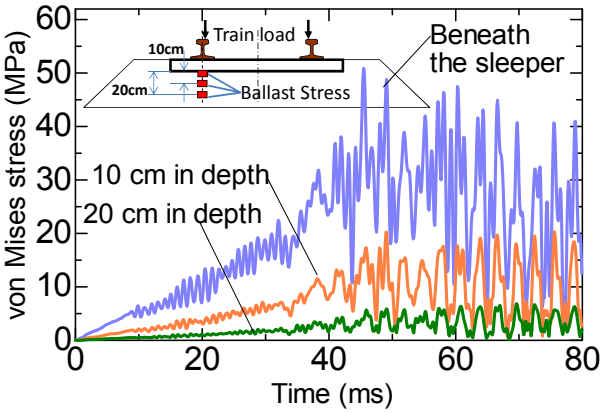

Figure 13: Time history of von Mises stress

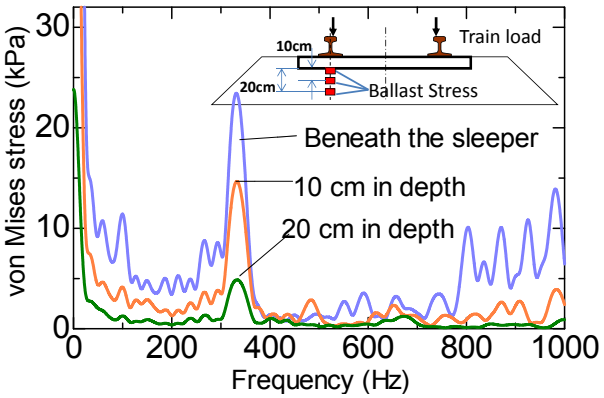

Figure 14: Spectra of von Mises stress

Figure 14 shows the linear amplitude spectra of response of von Mises stress, on the cross-section inside the gravel angularity acting at different depths below the loading point of the left rail, which are obtained by conducting by the fast Fourier transformation of these time history response waveforms and smoothing them at a bandwidth of 20 Hz. From the figure, these spectra curves identify the 1st order elastic vibration resonance mode of the ballast layer at around 337 Hz, where the whole ballast layer stretches vertically as an elastic body.

In this analysis, significant stresses up to 80 MPa are observed in tetrahedral elements near the contact part while the average maximum pressure on the ballast surface is 74 kPa. In this case, the stress acting on the angularity part is approximately 1100 times greater than the average loading stress on the ballast surface. Assuming that the unconfined compressive strength is 60 MPa at the angularity part of the ballast gravel, the application of a dynamic load of 55 kPa or more to the ballast-layer surface would cause minute fracturing or breakage around locations where the stress acting on the angularity part of the ballast gravel converges.

3.4 Amplitude spectrum of the vertical displacement regarding impact loading

To detect the exact frequency of the elastic vibration mode of the ballast layer, the author performed a numerical experiment (simulation) which simulates the impulse loading experiment by using a transient response analysis of the aforementioned large-scale ballast aggregate model. Figure 15 shows the amplitude spectra of the vertical displacement of the sleeper by applying a 0.1-ms square impulse loading waveform. The impulse loading to the left and right rails totals 100 kN. According to the impact loading numerical experiment, the results indicate that the rigid-body natural vibration mode occurs at around 310 Hz. The results indicate that the analytical natural frequency of the elastic vibration mode of the ballast layer fairly coincides with the above-mentioned measured one and that the frequency corresponds to 3-times the value of the measured natural frequency of the rigid-body mode.

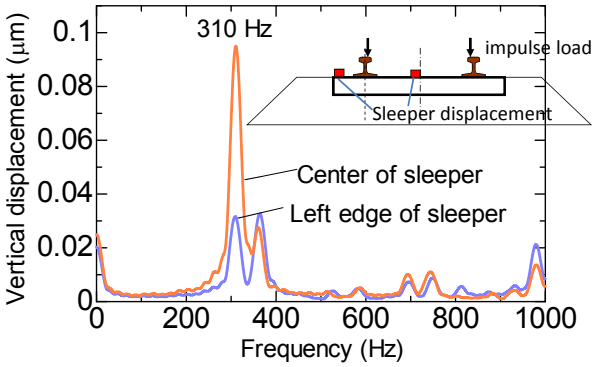

Figure 15: Response spectrum of vertical displacement regarding impulse loading

4 LARGE-SCALE FINITE ELEMENT TRANSIENT RESPONSE ANALYSIS REGARDING THE RIGID-BODY VIBRATION MODE

To examine the dominant rigid-body resonance motion observed at around 100 Hz, this chapter describes the large-scale finite element transient response analysis of the ballasted track by using the bilinear contact springs in place of the MPCs. According to the above-mentioned drop-weight test results, it is inferred that the ballast jumping motion, that is a rigid body bounce mode, causes large displacement. Therefore, regarding the aforementioned large-scale finite element ballasted track model, the contact-point information between the ballast pieces and the sleeper nodes is modeled with bilinear springs, that is, with tensionless contact. Table 3 shows the calculation parameters regarding contact points. In this analysis, the tension spring factors are

Table 3: Parameters of bilinear springs

Item	Compression spring factor (GN/m)	Tension spring factor (GN/m)
Ballast - Ballast	30	0.0003
Sleeper - Ballast	10	0.0001

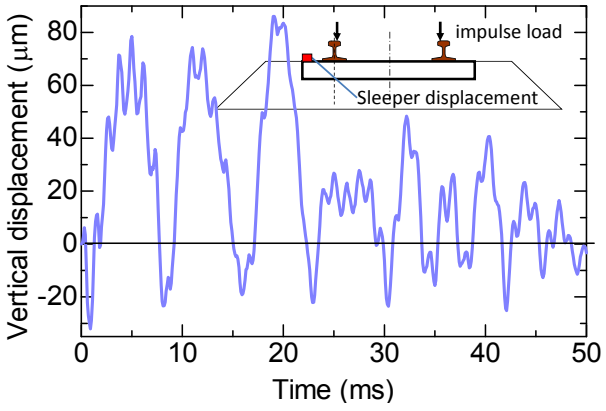

Figure 16: Time history of sleeper displacement

set at 1/100000 values of the compression spring factors.

Figure 16 shows the time history responses of the vertical displacement at the left edge of the sleeper immediately after the 0.1-ms square impulse loading waveforms of 100 kN. In this figure, the downward displacement means the downward motion of the sleeper (that is, the compression of the ballast layer), and the upward displacement means the upward motion of sleeper (that is, the extension of the ballast layer). According to the figure, when an impact load is applied, the ballast layer instantaneously deforms elastically due to compression and then returned to the pre-loading position. Thus, it takes only about 1 ms for the ballast layer to be compressed and be restored. Following the compression and restoration of the ballast layer, sleeper-jumping occurs. The cause for this sleeper-jumping is the strain energy stored in the ballast being released abruptly.

Figure 17 shows the amplitude spectrum of the vertical displacement of the sleeper. The results indicate that the rigid-body natural vibration occurs at 120 Hz. The value is approximately 10 - 20% larger than the experimental one. However, that is almost 1/3 of the elastic natural vibration frequency. According to the large-scale finite element analysis with nonlinear contact springs indicates that the rigid body natural vibration mode occurs almost at 1/3 of the elastic natural vibration frequency. It is inferred that the rigid-body natural vibration mode may occur at frequencies which are equal to the ones obtained by dividing the frequency of the elastic natural vibration mode by odd numbers.

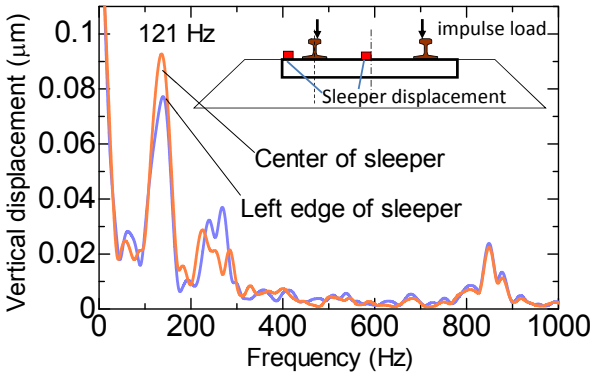

Figure 17: Vertical displacement regarding impulse loading

5 Discussion

When the contact-point information between the sleeper bottom and ballast pieces is modelled with MPCs, the vertical elastic natural vibration mode of the ballast layer numerically occurred at about 310 Hz. On the other hand, when the contact-point is modeled with nonlinear contact springs, that is, with tensionless contact, the rigid-body natural vibration mode is numerically detected approximately at 120 Hz. These analytical results coincide substantially with the ones obtained by the in-situ measurement and the full-scale experiment. Accordingly, the natural mode which occurs when an impact load is applied is mainly determined by the contact condition on the sleeper bottom.

As shown in aforementioned Figure 5, the amplitude of displacement of the ballast gravel decreases in inverse proportion to the squares of frequency according to the physical theory. Therefore, the occurrence of the rigid-body natural vibration at 1/3 of the elastic natural vibration frequency is expected to induce 9 times larger amplitude of displacement within the ballast structure than the elastic natural frequency. Therefore, the occurrence of the rigid-body natural vibration largely contributes to progress the deterioration of the ballasted structure. That is, in theory, the improvement of the contact condition between the sleeper bottom and

ballast layer can reduce the amplitudes of displacement to 1/9 compared with that in the current status of the ballasted track.

Figure 18 shows the structural dumping coefficient on the sleeper bottom in vertical direction regarding a 30-cm-thick ballast layer, which has been identified by the experimental modal analysis using the full-scale mockup and precise finite element analysis according to the reference (Sakai and Aikawa, 2012). The figure shows that the damping factor of ballasted layer has extremely strong frequency dependency. The ballast layer, in the high-frequency domain over 200 Hz, provides extremely high dumping functions for reducing the impact energy. However, the ballast layer is almost non-resistant subject to the low-frequency wave components of dynamic loads. The low-frequency load components are not damped, unless the ballast aggregate is fully constrained by an appropriate amount of uniform pressure from the surrounding area.

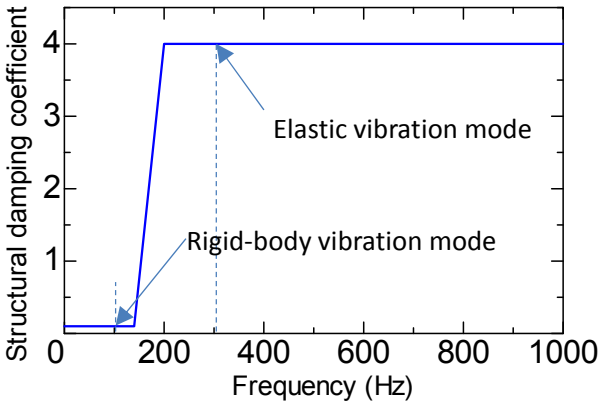

Figure 18 Structural damping coefficient of the ballast layer (Sakai and Aikawa, 2012)

Based on the above-mentioned mechanisms, the improvement of the contact condition adjacent to the sleeper bottom contributes to restrain occurrence of the rigid-body natural vibration resulting in a reduction of the ballast degradation.

6 CONCLUSIONS

In this paper, the author dealt with the vertical natural vibration modes of the ballast layer which lead to the phenomena of ballast deterioration, based on the precise field measurement, the full-scale experiments and the large-scale numerical analysis based on high performance parallel computing. The results can be summarized as follows:

(1) The impact loads by running trains induce the natural vibration modes within the ballast layer specific to the structure and consequently propagate within the ballast layer through motion in the natural vibration modes.
(2) The analytical results indicate that the stress acting on the angularity part of the ballast gravel is approximately 1100 times greater than the average loading stress on the ballast surface, and that the minute fracturing or breakage, around locations where the stress acting on the angularity part of the ballast gravel converges, occurs at any time due to regular train passage.
(3) The normal frequency of the vertical elastic vibration mode is numerically detected at around 310 Hz. The rigid body vibration occurs almost at 1/3 of the elastic vibration mode frequency. The result coincides substantially with the field measurement results. It is inferred that the rigid body vibration modes easily occur at frequencies which are equal to the ones obtained by dividing the frequency of the elastic vibration mode by odd numbers according to the amount of the overburden mass.

(4) The occurrence of the rigid-body modes of the ballast layers plays an important role in the progress of the ballast deterioration. Therefore, the improvement of the contact condition near the sleeper bottom contributes to reduce the displacement amplitude of ballast gravel resulting in a reduction of the ballast degradation.

REFERENCES

[1] Aikawa, A.: "Application of a Special Sensing Sleeper for Dynamic Interaction within the Boundary Layer between a Sleeper and Ballasts," *The 11th International Conference on Computational Structures Technology*, Paper No. 130, Civil-Comp Press, (2012).

[2] Aikawa, A., Urakawa, F., Abe, K., Namura, A.: "Dynamic Characteristics of Railway Concrete Sleepers using Impact Excitation Techniques and Model Analysis," *The 9th World Congress on Railway Research*, (2011).

[3] Aikawa, A.: "Assessment of the Dynamic Characteristics of a Ballasted Railway Track subject to Impact Excitation using Three-Dimensional Composite Finite Element - Discrete Element Modelling," *The 11th International Conference on Computational Structures Technology*, Paper No.137, Civil-Comp Press, (2012).

[4] CERFACS, ENS Lyon, INPT(ENSEEIHT)-IRIT, Inria and University of Bordeaux, "MUltifrontal Massively Parallel Solver (MUMPS 5.0.0) Users' guide", http://graal.ens-lyon.fr/MUMPS/, (2015).

[5] Grassie, S.L., Gregory, R.W., Harrison, D., Johnson, K.L.: "Modelling of railway track and vehicle/track interaction at high frequencies," *Vehicle System Dynamics*, 22 (3-4), pp.209-262, (1993).

[6] Okuda, H.: "Structural Analysis for Large Scale Assembly: Research and Development of Innovative Simulation Software," http://www.ciss.iis.u-tokyo.ac.jp/

[7] Railway Bureau, MILT (Ministry of Land, Infrastructure, Transport and Tourism, and Railway Technical Research Institute, Japan) and RTRI: "Design Standards for Railway Structures and Commentary (Track Structures)," Maruzen Publishing Co., Ltd., (2012), (in Japanese).

[8] Sakai, H. and Aikawa, A.: "Three-Dimensional Finite Element Analysis of Sleeper Vibration with the Influence of Ballast," *The 1st International Conference on Railway Technology: Research, Development and Maintenance*, Civil-Comp Press, (2012).

[9] Sakai, H. and Aikawa, A.: "Finite Element Vibration Analysis of Sleepers including Ballast Damping Characteristics," *International Journal of Railway Technology*, 1(3), pp.37-59, Civil-Comp Press, (2012).

[10] Urakawa, F., Aikawa, A., et al.: "Development of Remote Automatic Measuring System for Long-term Measurement of Dynamic Responses of Tracks," *Proceedings of Railway Mechanics*, No. 13, pp. 23-28, JSCE, (2009), (in Japanese).

[11] A. Aikawa, "Determination of the Natural Modes of a Ballast Layer", *Proceedings of the Ninth International Conference on Engineering Computational Technology*, Civil-Comp Press, No.19, (2014).